Experimental Investigation of Spray Characteristics of Pre-filming Air-blast Atomizers

M. Roudini[†] and G. Wozniak

Institute of Mechanics and Thermodynamics, Chemnitz University of Technology, Chemnitz, Germany

†*Corresponding author email: mehrzad.roudini@s2013.tu-chemnitz.de*

ABSTRACT

A bulk of a liquid dispersed into single droplets using the kinetic energy of a high-velocity gas in an air-blast atomizer is frequently employed in technical atomization processes. The atomized liquid is primary situated on a surface (prefilming surface) to form a thin liquid film before being exposed to high-velocity air flow. Moreover, the performance of spray processes is affected by the variation in the atomizer geometry, liquid physical properties and operational conditions. The purpose of this study is to examine and describe the influence of the nozzle geometry and a wide range of test conditions on the spray performance of prefilming air-blast atomizers. In order to evade the commonly complicated internal flow, an important but simple geometry was selected. Liquid break up mechanisms close to the atomizer exit were investigated using shadowgraphy associated with particle tracking. Furthermore, high-resolution local velocity and droplet size measurements were performed using phase Doppler anemometry (PDA). On the whole, the break up mechanism is considerably influenced by either air pressure and liquid flowrates or atomization edge size. Droplet size distribution profile of the different spray parameters in axial and radial directions are studied. The location of the maximum droplet mean velocity and the minimum Sauter mean diameter (SMD) within the spray are determined. The prefilming surface area and atomization edge size were observed to influence the liquid sheet breakup, droplet velocity and droplet size. With an atomization edge length increase of 5.7 mm, the global SMD increased to a maximum of 70% within different operation conditions.

Keywords: Spray characterization; Prefilming airblast atomizer; Liquid atomization; Phase doppler anemometry.

NOMENCLATURE

A	area	z	coordinate in radial direction
ALR	air to liquid mass flowrate ratio	μ	dynamic viscosity
d	characteristic length	ν	kinematic viscosity
d_e	outer diameter of tube	ρ	density
d_i	inner diameter of tube	σ	surface tension
D	gas slit diameter		
GSMD	global sauter mean diameter		**Subscripts**
$\dot{m}$	mass flow rate	a	air
N	nozzle number	b	breakup
p	pressure	e	outer
Re	Reynolds number	g	gas
SMD	sauter mean diameter	i	inner
U	velocity	l	liquid
$\dot{V}$	volume flow rate	p	prefilming
$\ddot{V}$	volume flux	r	relative
We	Weber number	n	normal conditions
x	coordinate in axis direction	rel	relative

1. INTRODUCTION

A bulk of a liquid dispersed into single droplets using the kinetic energy of a co-flowing high-velocity gas is widespread in many technical processes and practical applications. This common

type of atomization is generally referred to as air-blast atomization. Air-blast atomizers have many advantages over other types of atomizers, especially in their application to combustion systems operating at high pressure (Correa, 1993; Lefebvre & McDonell, 2017; Lefebvre & Ballal, 2010). For example, in spite of a complex atomization process, fine droplets are generated at a wide range of liquid flowrates in the early stages of atomization, which will improve mixing of spray and surrounding air (Ashgriz, 2011; Lefebvre & McDonell, 2017). The most common design of the air-blast atomizers is the prefilming atomizer, in which the atomized liquid is primary situated on a surface (prefilming surface) to form a thin liquid film before exposing to high-velocity air flow. The prefilming surface generates a thin liquid film before the liquid atomization which caused a finer spray compared to the non-prefilming design (Lefebvre & McDonell, 2017).

The spray production process exhibits two main phases. Initially, at the near field of the atomizer, the flow deformation and the following production of liquid fragments establish the primary breakup mechanism. Later, at the far field region, the liquid fragments may also be distorted and disintegrated into stable drops forming the secondary breakup mechanism (Lefebvre & McDonell, 2017). The primary phase has been often unnoticed and is still a topic of ongoing research (Gepperth et al., 2012; Gepperth, Koch, & Bauer, 2013). The secondary breakup of droplets is generally understood (Guildenbecher, López-Rivera, & Sojka, 2009; Hardalupas & Whitelaw, 1994; Urbán, Zaremba, Malý, Józsa, & Jedelský, 2017). However, the understanding of atomization mechanisms close to the atomizer exit, the detailed characteristics of droplet velocity, droplet size distributions, and concentration as functions of time and space, and prediction methods are essentially required for the development and design of prefilming air-blast atomizers.

The performance of any given type of atomizer depends on nozzle geometry, operating conditions, and the physical properties of the dispersed and continuous phases (Lefebvre & McDonell, 2017). The demanding challenge is to develop an atomizer in view of the rheological properties of the liquid to be atomized and the given process parameters in a spray along specific desired properties such as droplet sizes and velocities. Different atomizer designs were firstly studied and the comparisons of the droplet sizes were investigated in one single location (Liu, Li, et al., 2006; Rizk & Lefebvre, 1983). Even though there are few works available studying the influence of the prefilming surface in the simplified planar injectors (Bhayaraju, 2007; Gepperth et al., 2012). Indeed, one of the present study aims is to investigate the influence of the prefilming surface geometry and atomization edge length on the liquid breakup mechanisms close to the prefilming airblast atomizer and the generated spray profile.

The atomization process and breakup system of a wide variety of twin-fluid nozzle designs have been studied in various investigations. The liquid is generally discharged through an air-blast atomizer

in form of numerous small liquid jets or sheets. The first liquid jet theoretical model called Rayleigh breakup was developed by Rayleigh (Rayleigh, 1878). The effects of viscosity, aerodynamic forces, and drag forces on jet disintegration have been considered in later investigations (Haenlein, 1932; Weber, 1931). The liquid sheet breakup has been studied theoretically (Dombrowski & Johns, 1963; Hagerty & Shea, 1955; Mehring & Sirignano, 2004; Rangel & Sirignano, 1991; Xue et al., 2015) and experimentally (Arai & Hashimoto, 1985; Berthoumieu & Lavergne, 2001; Crapper & Dombrowski, 1984; Dombrowski & Fraser, 1954; Mansour & Chigier, 1995; Rizk & Lefebvre, 1980; Stapper, Sowa, & Samuelsen, 1992) and different modes of sheet disintegration have been suggested. The effect of air and liquid loading on the formation, size, and lifetime of ligaments have been investigated (Stapper et al., 1992). They concluded that the ratio of liquid-air velocity is an important factor in sheet and ligament breakup. It was observed that external forces reduce the thickness of the liquid sheet during breakup (Dombrowski & Johns, 1963). Experimental studies showed that the liquid breakup length decreases with an increase of the relative velocity between liquid jet and the streaming gas in air blast atomizers (Engelbert, Hardalupas, & Whitelaw, 1995; Lasheras, Villermaux, & Hopfinger, 1998; Yang, Cuoco, & Oschwald, 2007). However, as it was observed, liquid disintegration in pre-filming air-blast atomizers consists of many random breakup events due to different pressure areas close to the nozzle. Since little evidence is available for the breakup of a liquid sheet from a pre-filming surface and the influence of pre-filming surface on spray performance, high-speed photography is required to visualize the disintegration mechanisms, ligament breakup and spray formation in various atomizer geometries and operational conditions.

The droplet size is one of the most important aspect to characterize the spray in the far field region. The droplet size distribution is mainly modeled empirically and analytically by the existing literature (Babinsky & Sojka, 2002; Lefebvre, 1989; Liu, Gong, Li, Wang, & Yu, 2006; Sellens & Brzustowski, 1985; Urbán et al., 2017; Zhou & Yu, 2000). For a specific atomizer design, parametric analysis should be performed experimentally to attain empirical correlations between mean drop sizes and operating conditions. In a well-known correlation for the droplet diameter in an air-blast atomization, Rizk presented an empirical, dimensionally correct equation (Eq. (1)) which consists of two separate terms, one of which is dominated by the relative velocity and surface tension and the other by viscosity, given by (Rizk & Lefebvre, 1985):

$$\frac{SMD}{d_i} = 0.48\left(\frac{\sigma}{\rho_g U_{rel}^2 d_i}\right)^{0.4}\left(1+\frac{1}{ALR}\right)^{0.4}$$

$$+0.15\left(\frac{\mu_l^2}{\sigma\rho_l d_i}\right)^{0.5}\left(1+\frac{1}{ALR}\right) \tag{1}$$

where d_i is inner diameter of the liquid feeding tube, ρ_g is the gas density, U_{rel} is the velocity between air and the liquid jets at the exit, ALR is the air to liquid mass flow rate ratio ($\frac{\dot{m}_a}{\dot{m}_l}$), μ is the dynamic viscosity, σ is the surface tension and the Sauter Mean Diameter (SMD) is the diameter of the drop whose ratio of volume to surface area is the same for the entire spray. The SMD is a crucial parameter for mass transfer and combustion related applications of sprays (Lefebvre & McDonell, 2017). Later on, SMD was found inversely related to the relative velocity, gas-to-liquid momentum and mass flow ratio (Hardalupas & Whitelaw, 1994; Li & Shen, 2001; Rizk & Lefebvre, 1985). Leboucher, Laporte, Carreau, & Roger (2007) and Li & Shen, (2001) have investigated the spray resulting in the far field, the near field, and the midfield, of an annular liquid sheet with inner and outer gas co-flows, respectively. They found that the inner gas swirl slightly reduces the SMD but homogenizes the droplet velocities. Furthermore, the obtained SMD was constant in the central region and raised sharply as it reached the periphery of the spray. Equation (1) and the other investigated correlations are generally capable to explain the tendency of the SMD. However, they are rather valid for specific measurement positions and special cases. For a general description of the performance of pre-filming air-blast atomizers with different designs, the influence of the nozzle geometries and operational conditions on the droplet size distributions are reviewed by Gepperth (Gepperth *et al.*, 2013). Due to the complexity of most practical atomizer designs and difficulties in the manufacturing of atomizers, the present research is focused on an atomizer with a round liquid jet surrounded by an annular air channel. It represents a fundamentally simple but important geometry which is used to produce fine sprays especially for viscous liquids (Aliseda *et al.*, 2008).

In this paper, in addition to the variation of the nozzle geometry, the effects of air and liquid loading on spray productivities have been investigated. As spray liquid, conventional tap water has been used. PDA (Phase Doppler Anemometry) as the most sophisticated instrument employed in spray analysis has been applied. The development of the droplet size and velocity is inspected along the spray axis and spray radial direction. The spray axial distance with smallest and fastest droplets are determined which is an important parameter for different atomization applications. The effect of different parameters on the spray two dimensionalities has been investigated. Furthermore, the liquid film breakup process near the nozzle exit using high speed shadowgraphy has been carefully tracked to gain a better understanding of the liquid atomization process in that region.

2. EXPERIMENTAL SETUP AND MEASUREMENT TECHNIQUES

In this study, the experimental setup consists of three main sections, (1) atomizer, liquid and gas supply system, (2) background shadowgraphy, and (3) droplet sizing setup. The type of pre-filming air-blast atomizers investigated in the present study have been used before by (Glathe, Wozniak, & Richter, 2001). Important geometries and definitions are shown in Fig. 1. To avoid the complicated internal flows of most practical atomizers, a fundamentally important nozzle exit has been selected. Air-blast atomizers are designed and manufactured at the Suvis GmbH, Germany. The central tube inside diameter varies from 3.1 mm to 1.1 mm to study the influence of the inner liquid tube diameter and pre-filming surface area at constant air velocity. The outer liquid tube diameter increases from 2.6 mm to a maximum of 4.5 mm to study the effect of the atomization edge on the spray performance at constant liquid flow conditions. The exit of the air jet was manufactured with a diameter 5.6 mm, resulting in annular widths of 0.5, 0.8, 1.2 and 1.7 mm to investigate the pre-filming edge geometry impacts on the spray behavior.
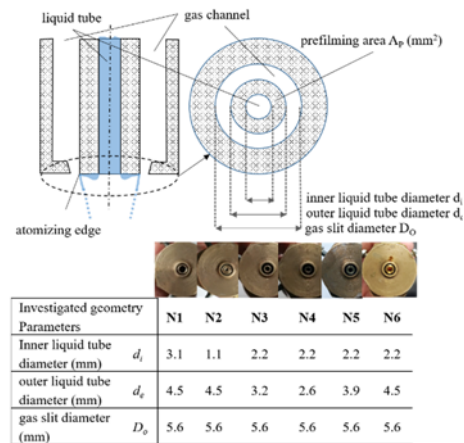

Investigated geometry Parameters		N1	N2	N3	N4	N5	N6
Inner liquid tube diameter (mm)	d_i	3.1	1.1	2.2	2.2	2.2	2.2
outer liquid tube diameter (mm)	d_e	4.5	4.5	3.2	2.6	3.9	4.5
gas slit diameter (mm)	D_o	5.6	5.6	5.6	5.6	5.6	5.6

Fig. 1. Investigated atomizer geometries.

The experiments were performed at ambient conditions where it is possible to perform flow visualization measurements and reliable Phase Doppler Anemometry (PDA) measurements. PDA is a non-intrusive optical measurement device which measures the size, velocity and concentration of spherical droplets flowing in air. The operating conditions of the PDA sizing measurements and flow visualization are summarized in Table 1. The important non-dimensional numbers in the atomization process such as the relative Weber number $(We_{rel} = \frac{\rho_g.(U_g-U_l)^2.d_l}{\sigma})$ and liquid Reynolds number $(Re_l = \frac{\rho_l.U_l.d}{\mu_l})$ which are shown in Table 1. ρ_l, ρ_g, σ, μ_l, U_l and d are the liquid density, gas density, liquid surface tension, liquid viscosity, liquid velocity, and characteristic length respectively.

A schematic of the experimental apparatus is shown in Fig. 2. The air was supplied to the nozzle by an in-house central oil free air compressor. Water was supplied using a pressurized liquid tank and the flow rate was adjusted by a valve before and after the flowmeter. The air and liquid are metered by an in-house assembled mass flow meter box. To

capture the relevant flow parameters, pressure and temperature probes were connected. The atomizers were positioned horizontally.

As shown in Fig. 3, in order to analyze the disintegration of the liquid near the nozzle exit, background shadowgraphy was implemented using a high speed intensified camera (Photron - FASTCAM SA5) to capture the images with a 256 x 256 pixel resolution at a rate of maximum 87500 frames per second and a maximum shutter speed of 1/1000000s. A long-time flash trigger unit, Drelloscop 1504, was used to illuminate the background of the spray. The camera was located on the opposite side of the flash lamp so that the shadow of the spray could be captured. The shadowgraphy images were analyzed
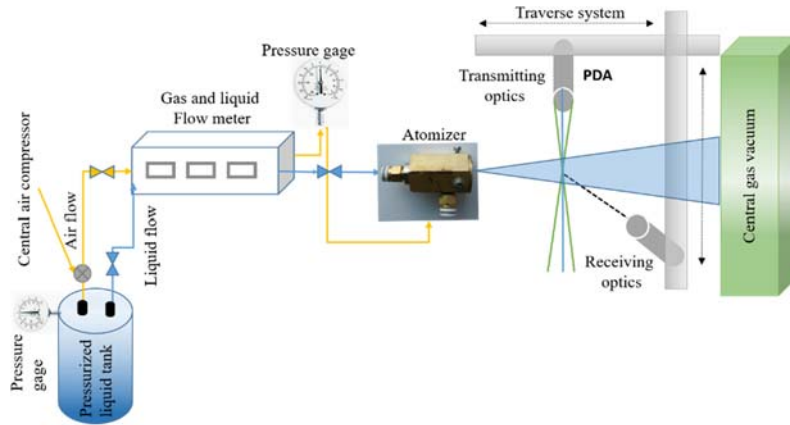
Fig. 2. Schematic of the experimental setup

Table 1 Experimental parameters and operation conditions

|	Air			Liquid			
PDA Measurement	P_{air} (bar)	$\dot{V}$ (nl/min)	We_{rel}	$\dot{V}$ (ml/min)	Velocity (m/s)	Re_l	ALR
Air/Liquid flowrates	0.25-1.5	38-133	71-224	10-150	0.04-0.63	99-1408	0.26-6.9
Nozzle geometries	0.20-0.60	33-70	35-443	30-90	0.06-1.57	204-1730	0.58-1.75
Flow Visualization	Air			Liquid			
	P_{air} (bar)	$\dot{V}$ (nl/min)	We_{rel}	$\dot{V}$ (ml/min)	Velocity (m/s)	Re_l	ALR
Air/Liquid flowrates	0.25-1.5	36-133	67-224	2-62	0.01-0.25	19-582	0.64-33.2
Nozzle geometries	0.05-0.72	17-79	8-512	5-80	0.01-1.40	34-1538	0.64-10.7
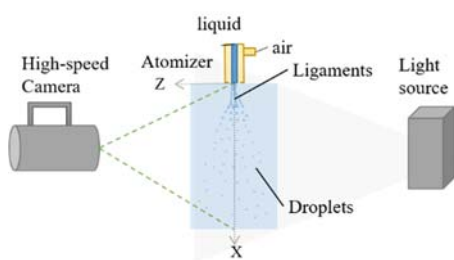
Fig. 3. Schematic of shadowgraphy technique setup

using a National Instruments vision assistant software. A script has been generated for the different structure parameters including a series of image processing steps, analysis functions, and the related parameters at each step (Fig. 4). After image calibration, which is shown in step 1 in Fig. 4, filters are required to prepare the images for processing. First, a lookup table was applied to improve contrast and brightness of the images. A convolution kernel with size 3 highlights the edges of the image. In the next tab, a gray morphology function was applied to delineate objects and prepare images for thresholding and quantitative

analysis in step 2. In the next step, threshold operations enable to select ranges of grayscale pixel values. The manual thresholds have been chosen since uniform lighting changes from image to image were not expected. After thresholds, a binary function called basic morphology improved the shape of the particles in the binary image by smoothing the boundary of the particles, filling small holes in the particles, and closing small gaps along the perimeter of the particles. In this step, a particle filter was required to remove or keep particles in an image as specified by the filter criteria. In the final step, a particle analysis was performed to analyze the properties of the remaining particles (ligaments and droplets) regarding sizes and positions in the image (step 4).

For spray analysis, PDA as a non-invasive local measurement technique was applied which allows to measure the size, velocity and concentration of droplets in sprays. The phase difference of the Doppler frequencies measured by multiple detectors located at different angles provided the size of the droplets. In the present study two-component

measurements were performed by a Dantec Dynamic PDA based on conventional optics and a signal processor to characterize the velocity field and spherical particle sizes of the flow downstream of the atomizer. The scattering angle was adjusted to 43 degrees. The PDA optical settings are given in Fig. 5. More details about the PDA technique can be found in (Albrecht, Damaschke, Borys, & Tropea, 2013), for example.

Since the evolution of the spray just in front of the atomizer is essential for different applications especially in the combustion chambers, the development of the droplet size and velocity is required to be inspected along the spray axis and radial direction. The coordinate system for the PDA measurements is shown in Fig. 5. As given in Fig. 5, point investigations made at plane A ($x = 20$ mm, $y = -6$ mm to $+6$ mm, $z = -6$ mm to $+6$ mm) with 13 measurement points, plane B ($x = 50$ mm, $y = -8$ mm to $+8$ mm, $z = -8$ mm to $+8$ mm) with 17 measurement points, plane C ($x = 100$ mm, $y = -15$ mm to $+15$ mm, $z = -15$ mm to $+15$ mm) with 21 measurement points and lastly plane D ($x = 150$ mm, $y = -18$ mm to $+18$ mm, $z = -18$ mm to 18 mm) with 25 measurement points. Furthermore, the measurement locations were set along the centerline from $x = 5$ mm to $x = 200$ mm with 40 measurement points to observe the spray quality in different axial distances from the nozzle.
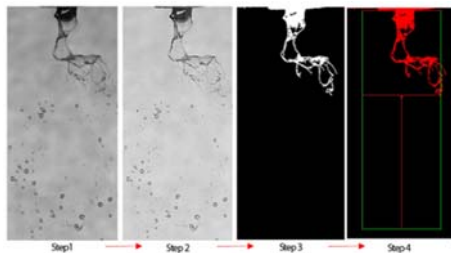

Fig. 4. Image processing steps of breakup length measurements

The selected measurement matrix points can validate the spray two dimensionalities near and far from the nozzle and provide detailed local measurements for characterizing the SMD and the dispersion of the spray.

Raw data from the PDA software (BSA Flow V.5.2) were exported and the statistical analysis and the data assessment were performed separately using the software OriginPro.

The uncertainty of the air volume flowrate was ±3% and of the liquid mass flow less than 0.5%. The images have been acquisitioned with 256*592 pixel resolution to be able to track the high-speed liquid ligaments. The uncertainty in the breakup length measurement is estimated by changing the threshold value used in the image processing algorithm. The calculation of a breakup length exhibited a standard deviation up to 28% of the mean due to the instability of the liquid atomization process. During PDA measurements, the valid data quantity of PDA was set to 10000. A high-resolution measurement is performed to reduce the uncertainty of the measurement locations. For the PDA measurement,

the maximum uncertainties on the droplet velocity
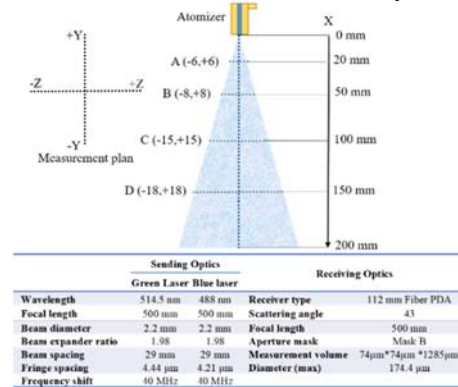
**Fig. 5. PDA measurement locations and optical setting**

and diameter measurements were both ±2% and the maximum tolerance for the sphericity validation was 10%. (see (Dantec Dynamic A/S, 2014) for more information). Eventually, the manufacturing tolerances of the characteristic nozzle dimensions were ± 0.01 mm.

3. EXPERIMENTAL RESULTS AND DISCUSSION

3.1 Flow Visualization

At the beginning, the liquid breakup and spray pattern close to the nozzle orifice were investigated in a wide range of air and water flowrates. It was observed that the interactions between air flow with the surfaces of the liquid structures, namely sheet, ligaments and droplets, produce different breakup regimes at various operating conditions. Eventually, the liquid breakup mechanisms have been investigated in detail on each nozzle geometry.

The spray pattern in the vicinity of the nozzle exit showed frequently a consistent three zones breakup constellation in experimental observations, Fig. 6. Zone I consisted of a conical liquid core which developed by aerodynamic forces close to the atomizer. At low liquid flowrates, the front face of the liquid tube performs as a pre-filming surface, where the liquid spreads out initially in a thin continuous sheet to wet radially the pre-filming surface. The liquid emerges from the feeding liquid tube and spreads out in a thin continuous sheet in the radial direction due to the low pressure area in front of the prefilming surface. It was observed that the liquid expanded until a critical flow condition was reached. After that, the lamella disintegrates
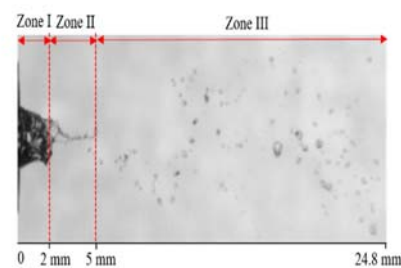

Fig. 1. Spray pattern close to atomizer

immediately using the momentum energy of the high-velocity gas. The breakup mechanisms in zone II were detected to contain randomly both well-known liquid jet and liquid sheet breakup mechanism due to strong interaction with the high-speed air. The co-flowing air provides the essential shear stress to strip ligaments as small jets from the outer surface of a continuous liquid core extending

from the pre-filming edge. These phenomena occurred mostly in high momentum air operations. The exact location of the border is highly dependent on the air/liquid flow rates and the nozzle geometry. These two unstable zones are termed in the literature as primary breakup. The secondary breakup regime begins in zone III where the larger droplets have undergone a secondary atomization due to aerodynamic – shear instabilities generating small droplets.

In the spray characterization investigation, the location of the completed secondary atomization and fully developed spray region has been determined in detail using local high-resolution droplet size measurements. The borders of the zones change their location during different experiments. These processes are in satisfying agreement with findings of previous studies (Glathe *et al.*, 2001).

Figure 7 shows the influence of air static pressure and liquid loading on the liquid disintegration. Figure 7 - (a) reveals that an increase in the liquid flowrate influences significantly the spray of zones I and II. It forms a conical core region and ligaments larger near the atomizer and the breakup take longer to process. However, the captured photos reveal that the liquid flowrate has less effect
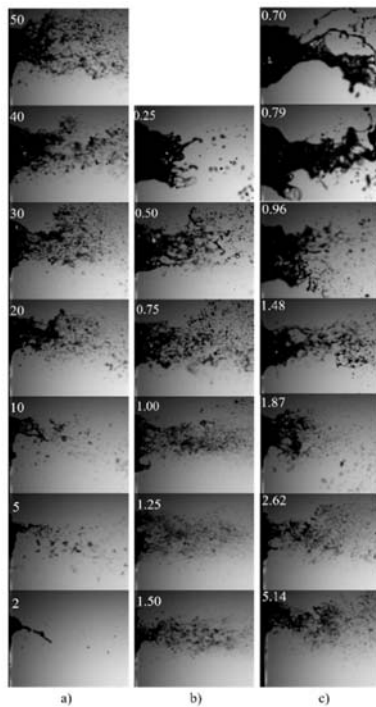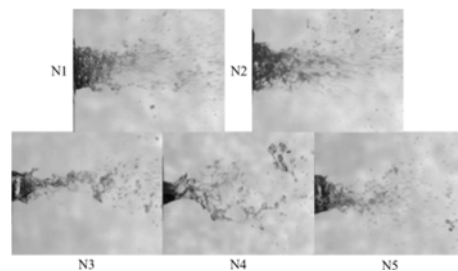
on the droplet size downstream of the nozzle. Since the pre-filming area is not fully wetted for $\dot{V}_1 < 20$ ml/min and the liquid film shaped at the atomizing edge is not uniform, it consequently influenced the symmetrical nature of the breakup process near the nozzle exit. Figure 7 - (b) shows the air pressure effect on the breakup process. As P_{air} increases from 0.25 bar to 1.50 bar, the initial ligaments and droplets become shorter and the breakup occurred close to pre-filming edge. The droplets are formed in the area interacting with higher air momentum; accordingly, the droplets became smaller downstream of the spray. However, a strong recirculation area was clearly observed from the experiments with $P_{air} > 1$ bar due to a high turbulence intensity close to the nozzle orifice. The air to liquid mass ratio (ALR) influenced the breakup mechanism in the same manner as the air velocity in all three zones as shown in Fig. 7 - (c). As ALR increases from 0.7 to 5.1, the liquid atomization takes a shorter time to progress. Zone I with the liquid conical core disappeared in case of ALR 2.6 and 5.1. The breakup mechanism and ligament size are influenced tremendously by ALR at zone II. The pre-filming area is only fully wetted for ALR 0.96 and lower (Fig. 7 - c).

The liquid breakup mechanisms of the 5 nozzles with same air pressure and liquid loading (P_{air} 0.4 bar /$\dot{V}_1$ 80 ml/min) are presented in Fig. 8. The water disintegration in N1 and N2 revealed a very familiar model of the atomization close to the atomizer. The inner liquid discharge orifice diameter displayed a very small effect on the breakup mechanism. It could be due to the equivalent air channel annular thickness which generates the same air momentum at the atomization edge. However, the atomization edge influenced the atomization model significantly in nozzle 3, 4 and 5 especially in high air velocity operating conditions.

N4 has nearly no pre-filming area (smallest atomization edge) and thus the smallest contact area between air stream and liquid flow. It produces a lower air velocity when leaving its air channel. Hence, larger ligaments and droplets were observed near the nozzle exit. The larger droplets will affect the droplet size distribution in the spray and it reduces the spray efficiency in most applications, especially in combustion processes. Nevertheless, N5 with 3.9 mm outer liquid tube diameter disintegrated the liquid in shorter time, which is helping to produce smaller ligament in zone II and smaller droplets in zone III.

Fig. 2.Effect of spray processes on the breakup and spray pattern (Record Rate [fps]: 40000 - Shutter Speed [s]: 1/1000000)

Fig. 3. Effect of nozzle geometry on the breakup and spray pattern breakup (Record Rate (fps): 40000 - Shutter Speed(s): 1/1000000)

To model the liquid breakup of a pre-filming atomizer, the breakup length is one of the most important parameters to investigate. The length of the continuous portion of the jet, measured from the nozzle to the longest breakup point where drop formation occurs, is defined as breakup length (Lefebvre & McDonell, 2017). Figure 9 shows the measured breakup length and comparison among different spray parameters. Error bars represent the standard deviation within the measured time intervals. The breakup length measurement was challenging, since the instantaneous breakup position is not fixed during the atomization process. Therefore, an image processing algorithm has been developed and applied for the about 480 images of each test case. Figures 9 – (a), (b) show an increase of the breakup length with the air pressure decrease or a liquid flowrate increase. An air pressure increase from 0.25 bar to 1.5 bar with a constant water flow rate (20 ml/min) generated nearly a 2.7 mm reduction in the breakup length. The breakup length first drastically decreases with increasing air pressure and seems to converge to a level where a further increase in air pressure will only have a minor effect on it. Water flowrate variations (5 - 50 ml/min) at fixed air pressure (1 bar) caused breakup length changes from 1.2 mm to 4.0 mm. As it is observed, the breakup length is strongly dependent on the air pressure with $L_b \sim P_{air}^{-0.67}$, however, the liquid flowrate

dependency is $L_b \sim \dot{V}_l^{0.39}$ for $P_{air} = 1$ bar.

Nozzle geometry effects on the breakup length are also shown in Fig. 9 – (c). In the same operating condition, the shortest breakup length belongs to N2 and the longest N4. With comparison between N1 and N2, it is observed that the pre-filming area has a noticeable effect on the breakup length. The flowing liquid on the larger pre-filming surface helps to reduce the liquid film thickness before the disintegration process at the atomizing edge takes place. The small liquid film thickness causes the breakup to occur faster near the atomizer. By comparing the N3, N4 and N5 results, it is found that increasing the atomization edge perimeter while keeping the liquid tube constant, reduced the breakup length. The larger atomizer edge not only increases the contact surface between the atomizing liquid and air, but also generates higher air velocities in the air exit channel. Both phenomena reinforce the liquid film to be disintegrated faster.

From the experimental results an empirical equation was derived for the prediction of average liquid breakup lengths generated by prefilming airblast coaxial atomizers using the liquid Reynolds number and gas Weber number as follows:

$$\frac{L_b}{d_i} = 1.483(We_{rel})^{-0.41}(Re_l)^{0.36} \tag{2}$$

The influence of the relative Weber number in the proposed correlation agrees well with the correlation obtained by Eroglu (Eroglu & Chigier, 1991). Though, the Reynolds number dependency is smaller. It could be due to the used smaller liquid flowrate range or bigger liquid tube diameter in the current study.

3.2 PDA measurements

High-resolution PDA measurements were performed both radially and axially in order to analyze spray properties downstream the nozzle. The results of different operating conditions on spray characteristics are discussed in some detail. The effects of the geometrical parameters of the atomizer were investigated.

3.2.1 Influence of Operational Conditions

As it has been revealed in previous studies (Avulapati & Rayavarapu Venkata, 2013; Hardalupas & Whitelaw, 1994; Jedelsky, Otahal, & Jicha, 2007; Lefebvre & McDonell, 2017), drop size and velocity are significantly dependent on the input air pressure and ALR. However, the liquid flowrate has a weaker effect on the spray performance in air-blast atomization. In this study, high-resolution PDA measurements were conducted along radial and axial directions in order to understand the spray dynamics and to observe the influences of different parameters on the spray performance of the atomizers under investigation.

Generating a symmetric spray from an atomizer is critical in many practical applications. The volume flux, SMD and mean velocity profiles of the liquid droplets in the radial direction of an atomizer can
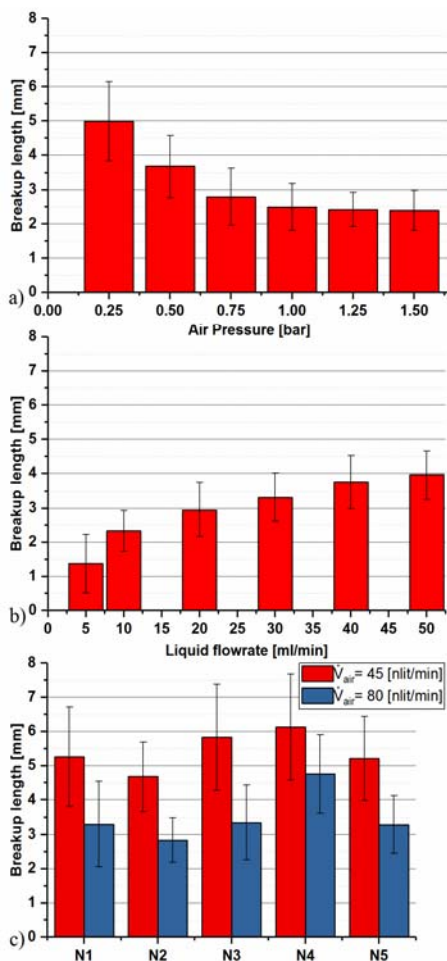

Fig. 4. Influence of air pressure (a), liquid flowrate (b), and nozzle design (c) on breakup length

support two dimensionalities of the spray with respect to its cross section. The volume flux presented here is the volume of liquid particles passing through a reference area in the axial direction per unit of time. Therefore, the influence of different parameters on two dimensionalities of the spray has been investigated. Air pressure and liquid flowrates influence the volume flux, SMD, and mean velocity along the radial direction as documented for N5. The plane in x = 100 mm axial distance has been selected. The reason is that the secondary atomization in x = 100 mm axial distance is completed and the droplets are no longer accelerating and the spherical nature of large droplets remains unchanged.

Radial direction: Details of the influence of the air pressure variation with a constant liquid flow rate of 50 ml/min are illustrated in Fig. 10. Figure 10 - a shows a symmetric trend of the volume flux distribution with an obvious local maximum on the nozzle center axis for the experiments with air pressure more than 0.75 bar. In low air pressure operation conditions specially at 0.25 bar, the volume flux distribution is almost flat along radial direction. The maximum volume flux in the center is increasing with the increasing of the air pressure due to higher numbers of the droplets, however, the volume flux reaches to a maximum amount at P_{air}= 1 bar in the location of 100 mm far away from the atomizer orifice. It could be due to evaporating of very small droplets at P_{air}= 1.5 bar. As Fig. 10 – a illustrates, spray width becomes significantly thinner with increasing air pressure. A symmetric radial profile of the mean velocity is observed with its maximum on the spray axis (Fig. 10 - b). However, there is a small shift of approximately 3 mm in high air pressure measurements like in the SMD distribution at the +z direction. This shift should be caused by the generated high-pressure region at the front of the atomizer. As Fig. 10 - c shows, the radial profile of SMD at lowest air pressure of 0.25 bar is almost flat. When the air pressure increases, the SMD value in the entire radial profile decreases mainly near the nozzle axis. From an air pressure of 0.5 bar on, the profiles tend to be inversely bell-shaped with their minimum on the spray axis and a small shift of the symmetric axis to the + z direction.

Details of the influence of the liquid flowrate are illustrated in Fig. 11. For a constant air pressure of 1 bar, an increase of the liquid flowrate leads to a slight increase of the droplet size and a small decrease of the droplet velocity in the central region of the spray. The SMD radial distribution changes its tendency with increasing liquid flowrate from bell-shaped to a flat line. The results show that with increasing liquid flowrate, a higher volume flux appeared mostly in the spray center. The volume flux profile shows a nearly symmetric distribution along radial direction in all liquid flowrates.

The influence of ALR on SMD, mean velocity, and volume flux distribution along radial direction is shown in Fig. 12. It is observed from Fig. 12 – a that the volume flux is very low in ALR values of 0.28 and 6.83. The maximum volume flux
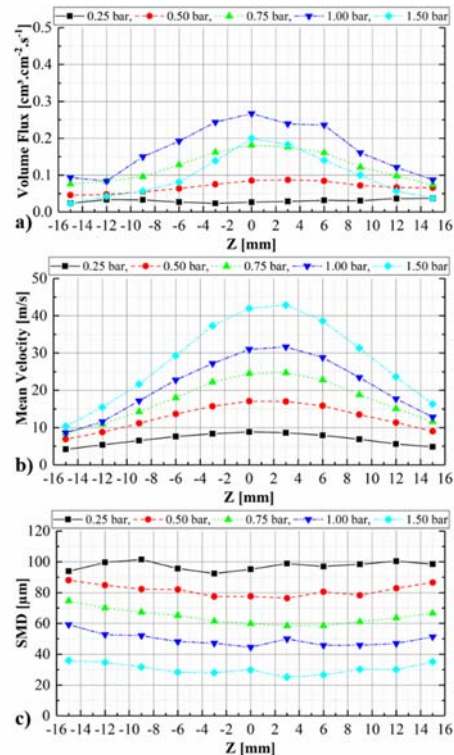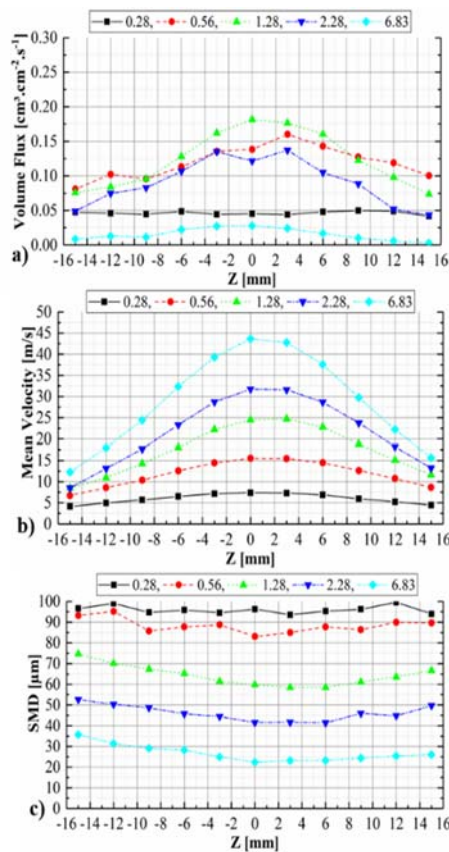

Fig. 10. Influence of air pressure on a) volume flux, b) mean velocity, and c) SMD distribution along radial direction.
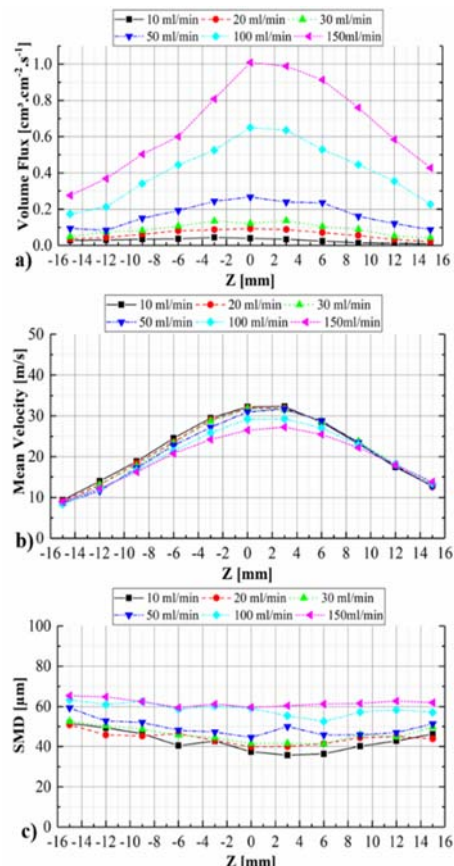
Fig. 11. Influence of liquid flowrate on a) SMD, b) mean velocity, and c) volume flux distribution along radial direction

appears in ALR 1.28 which is distributed almost symmetrically in radial direction. The droplets

Fig. 12. Influence of ALR on a) volume flux distribution, b) mean velocity, and c) SMD along radial direction

mean velocity increases and the SMD decreased significantly with increasing ALR especially in the center region of spray. The smallest SMD value of 22.36 μm and the highest velocity of 43,66 m/s at x = 100 mm and z = 0 mm, are achieved with maximum ALR of 6,83. The SMD shows a symmetric trend in all tests, however from ALR 1,28 on the SMD distribution reveals a bell-shaped tendency along radial direction.

Axial direction: The spray dispersion along the central axial direction should be known, as this will affect the volume flux distribution in a plane perpendicular to the flow direction and affects the spray global properties. The variation of the mean droplet velocity along the centerline of the spray cone for different air pressure, liquid loading and ALR is reported in Fig. 13.

Generally, the velocity increased along the centerline initially at 20 mm distance from nozzle tip. In this region, liquid film and the ligaments are provoked by air momentum forces and thus the velocity increases to a maximum amount in any operational conditions.

The liquid droplets are accelerating in this region, which will affect the spherical nature of large droplets and consequently the PDA measurements. From nearly 20 mm distance, the velocity decreases away to the x = 200 mm position. During this

distance, smaller droplets collide and form larger droplets, then lose their momentum due to drag. Thus, the droplet velocity starts decreasing away from the atomizer. As shown in Figs. 13 a and c, increasing air pressure and ALR have direct influence on the mean droplet velocity along the centerline. However, the liquid loading has less effect on the droplet velocity in the centerline axis specially at the downstream of the spray (Fig. 13 - b). Hence only the air momentum played a major role to determine the droplet velocity downstream of the evaluated atomizer.
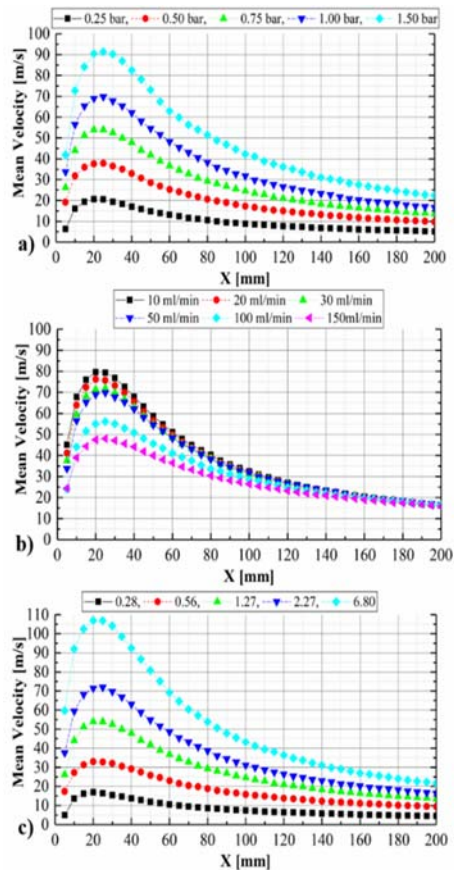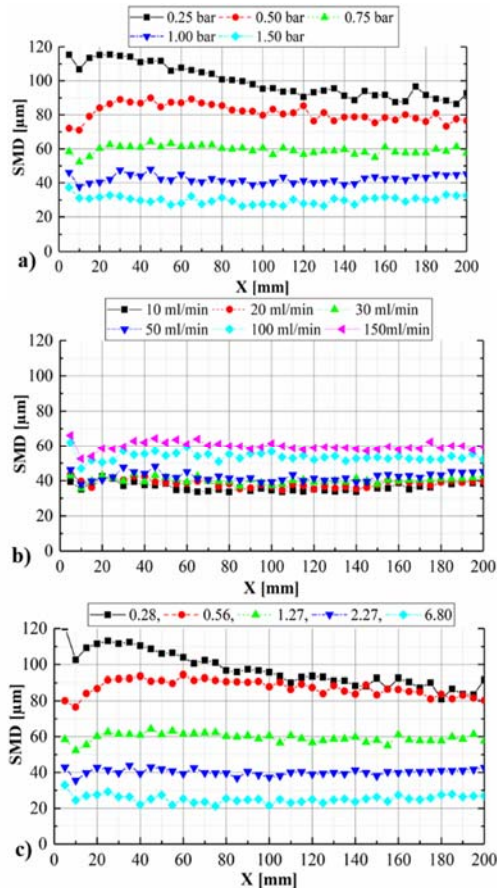

Fig. 13. Influence of a) air pressure, b) liquid flowrate, and c) ALR on mean droplet velocity along axial direction

In Fig. 14, the influence of air pressure, liquid loading, and ALR on SMD along axial direction from N5 is illustrated. Usually, the SMD axial profile includes four different regions during a spray.

In the first region, SMD increased dramatically from the nozzle tip along the centerline until a maximum SMD which is located between x = 20 mm and 40 mm. In the second region, a secondary atomization causes that the SMD reduces gradually to a constant quantity which belongs to a developed spray area. The smallest generated SMDs appeared in the region of x = 60 mm and 200 mm during the current experiments which is extremely dependent on the operation conditions. This area represents an important region with minimum SMD regarding spray applications. In the last region, SMD

commences to increase due to the evaporation of small droplets downstream the spray.

Figure 14 - a obviously shows the crucial role of the air momentum in the atomization using air-blast atomizers as also reported by other researchers (Lefebvre & McDonell, 2017). It reveals that increasing air pressure reduces SMD in the whole spray area. The area with smallest droplet size for air pressure 1.5 bar is attained faster at x = 60 mm and SMD starts to increase at x = 130 mm. Hence,


Fig. 14. Influence of a) air pressure, b) liquid flowrate, and c) ALR on SMD along axial direction

the smallest SMD region during air pressure investigation observed SMD range between 26 μm and 28 μm and a length of 70 mm at P_{air} = 1.5 bar. As can be observed from Fig. 14 - b liquid flowrate increase with constant air generates larger droplets, consequently, the developed spray appears in the area far away from the nozzle tip with having smaller air momentum. Figure 14 – c shows that an increase of ALR similar to air loading leads to a decreasing SMD in the entire axial profile.

Figure 15 shows the effect of air pressure and liquid flowrate on a global SMD. A global SMD (GSMD) is local volume flux weighted average of local SMD along two Y and Z axis of the spray. Each measurement using each atomizer has a single GSMD for a better comparison and it can be determined by Eq. (3) at any distance from the atomizer.

$$GSMD_z = \frac{\sum_{z=i}^{z=n} \ddot{V}_i . SMD_i}{\sum_{z=i}^{z=n} \ddot{V}_i} \tag{3}$$

Figure 15 - a shows tendencies as an increase of the GSMD with the liquid flowrate increase. Water flowrate variations (5 - 150 ml/min) at three different air pressures of 0.5, 1 and 1.5 bar reveal same trend in a GSMD increase. As it is shown in the Figure 15 – a, the GSMD is dependent on the liquid flowrate with GSMD $\sim \dot{V}_l^{0.1}$, $\dot{V}_l^{0.16}$ and $\dot{V}_l^{0.18}$ for air pressures of 0.5, 1 and 1.5 bar. However, the air pressure dependency is GSMD $\sim P_{air}^{-0.82}$, $P_{air}^{-0.82}$ and $P_{air}^{-0.68}$ for liquid flowrate of 10, 50
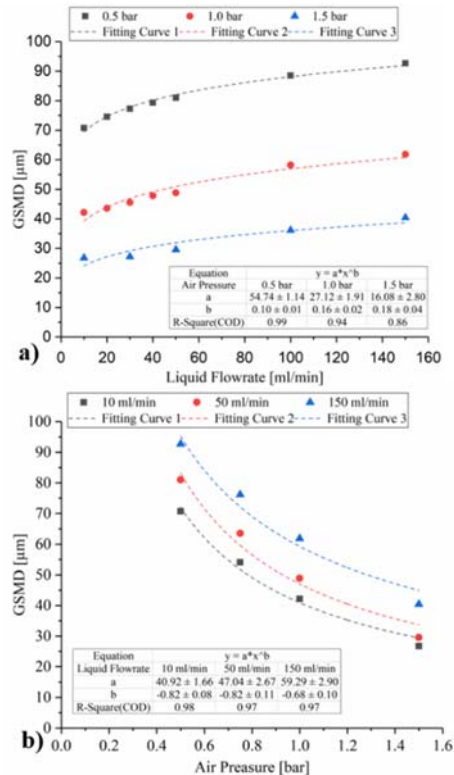
Fig. 15. Effect of (a) air pressure and (b) liquid flowrate on the GSMD

and 150 ml/min, respectively. It can be observed that increasing liquid flowrate reduces the dependency of air pressure on the GSMD in airblast atomizers.

An air pressure increase from 0.25 bar to 1.5 bar with a constant water flow rate (20 ml∕min) generated nearly a 2.7 mm reduction in the breakup length. The breakup length first drastically decreases with increasing air pressure and seems to converge to a level where a further increase in air pressure will only have a minor effect on it.

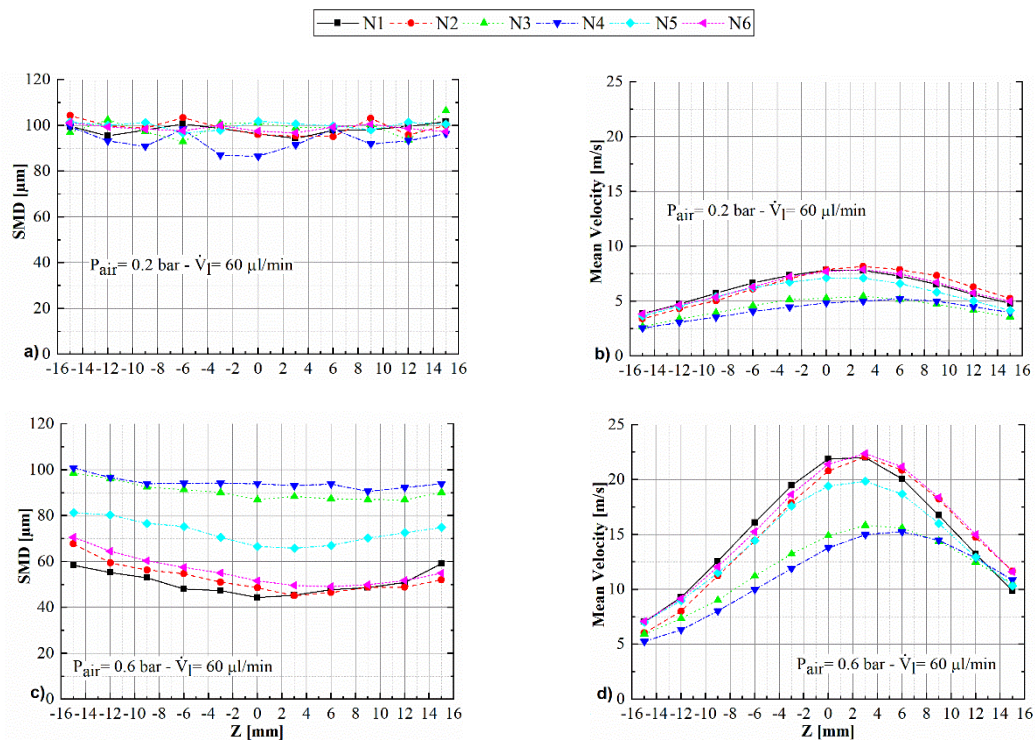### 3.2.2 Influence of Nozzle Geometry

The influence of two for the low flowrate liquid disintegration process, significant geometrical parameters, namely the outer liquid tube diameter (the atomizing edge diameter) d_e and the pre-filming area A_P have been studied in these experimental investigations, see Fig. 1. The PDA measurements were conducted at the same locations for the different atomizers. The influences of the

operation conditions have also been investigated at different pre-filming air blast atomizers. The evaluated operation conditions are listed in Table 1.

Radial direction: Details of the velocity and SMD profiles for the six different atomizers at two operation conditions at 100 mm distance from the nozzle exit are illustrated in Fig. 16.

As Fig. 16 – a shows, the SMD distribution is almost flat along radial direction at very low air pressure (P_{air} = 0.2 bar). The SMD fluctuates between 90 μm and 100 μm for all atomizers with a minor difference along radial direction. However, the faster droplets appeared in the spray center

shown in Fig. 16 – b. The mean velocities are symmetric across the z-axis for N1, N2, N6 with a small shift (2-3 mm) to +Z direction. Interestingly, N3 and N4 with a smaller prefiling area shifts the maximum droplet velocity 6 mm to the +Z. In higher air pressure (P_{air} = 0.6 bar) investigations, the mean droplet velocities increase with a similar tendency shown at Fig. 16 – d. N1, N2 and N6 with the same atomization edge generate smaller droplets (45 μm to 55 μm) in the center of spray due to higher droplet velocity and therefore higher aerodynamic forces in this region. Droplet sizes are increasing around the centerline to nearly a maximum of 70 μm at z = -15 mm. Increasing air

Fig. 16. Influence of the nozzle geometry on SMD (a, c) and droplet mean velocity (b, d) along radial direction.

pressure has a minor effect on droplet sizes using N3 and N4 with a very small atomization edge length. Indeed, the atomization edge length plays an important role to provide a wide range of the droplet sizes.

Axial direction: Details of the velocity and SMD profiles for the six different atomizers at two operation conditions within 200 mm from the nozzle exit are illustrated in Fig. 17.

The SMD variations within different atomizer designs in a low air pressure condition shows the same trend for all atomizers (Fig. 17 – a). Droplet sizes in the spray developed-area from different atomizers are fluctuating around 90 μm. However, N4 with smaller atomization edge interestingly generates slightly smaller droplets along axial direction. As Fig. 17 – b shows, N4 generates also slower droplets compare to the other atomizers which cause the smallest air and liquid velocity difference. A lower air and liquid relative velocity leads N4 to generate the smallest droplet size along

the spray centerline axis.

The velocity variations showed an identical trend for different atomizer designs. When comparing the droplet velocity variation between N1, N2 and N3 in a low or high air flowrate experiment (Figs. 17 – b and d), it is observed that N1 with smaller pre-filming area generated slightly faster droplets compared to N6 and later to N2. Consequently, a larger prefiling surface generated a larger wake region in the front of the atomizers and it reduces the velocity of the atomized liquid droplets. N5 with a bigger d_e causes a higher air velocity and accordingly a higher liquid droplet velocity along the axial direction in comparison with N3 and N4.

N1 with a larger atomization edge generates a wider droplet size range in the entire centerline axis especially in the minimum droplet size area (shown in Figs. 17 – a and c). However, the droplet size range is significantly small in N4. Consequently, the atomizing edge diameter (d_e),

which influences directly the air velocity, is an important parameter to increase considerably the droplet size range.

In Figs. 18 – a and b, the influences of two different nozzle geometries, the prefilming area and the atomization edge length, on the GSMD at 100 mm distance from the atomizer orifice are shown.

As can be seen in Fig. 18 – a, the GSMD is almost similar quantity in the air pressure of 0.4 bar and

0.6 bar for N1 and N2. However, N6 generates larger droplet sizes compared to N1 and N2. It was earlier noticed that a larger prefilming area creates a slightly lower droplet velocity, the lower aerodynamic force resulting in the larger droplets size. However, it is known from the literature that prefilming surface causes thinner liquid films and consequently smaller droplet sizes at prefilming airblast atomizers (Lefebvre & McDonell, 2017).
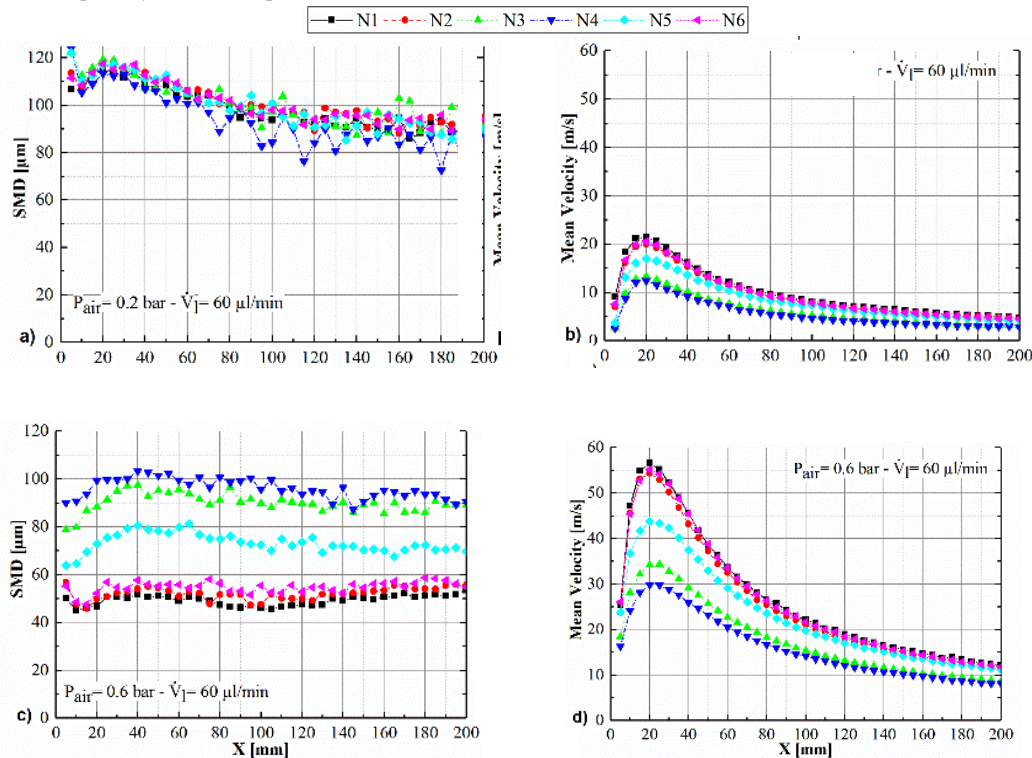

Fig. 17. Influence of the nozzle geometry SMD (a, c) and droplet mean velocity (b, d) along axial direction

As it can be observed from Fig. 18 – b, the atomization edge length plays an important role to produce a wide droplet size range. N4 with 8.3 mm atomization edge generates droplets from 93 μm to maximum 98 μm at 100 mm distance from the atomizer, however, N6 with 14.1 mm atomization range generates droplets from 55 μm to 99 μm. The wider droplet size range belongs to N1 with a droplet size range between 50 μm and 98 μm.

5. SUMMARY AND CONCLUSIONS

The effects of air pressure, liquid flowrates, atomizing edge length, and pre-filming area on the spray characteristics of pre-filming air-blast atomizers have been investigated. For that a high-speed ligament/particle tracking and a high-resolution particle size measurement technique have been applied. An algorithm has been developed to analyze liquid ligaments and particles close to the nozzle exit during various operational conditions. The results show that the liquid conical core region, ligament formation and breakup length are significantly dependent on liquid flowrate and air

pressure near the nozzle exit. As it is observed, the breakup length is strongly dependent on the air pressure with $L_b \sim P_{air}^{-0.67}$, however, the liquid flowrate dependency is $L_b \sim \dot{V}_l^{0.39}$ for $P_{air} = 1$ bar. From the experimental results an empirical equation was derived for the prediction of average liquid breakup lengths generated by prefilming airblast coaxial atomizers using the liquid Reynolds number and gas Weber number as shown in Eq. (2).
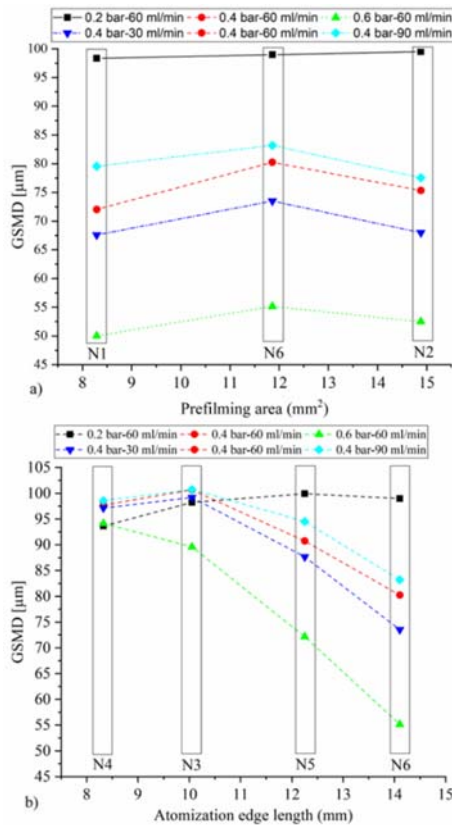
The results indicate that the pre-filming area is only fully wetted in ALR 0.96 and lower. Hence, the spray shows a symmetric behavior in the downstream direction of the spray. It turned out that the atomizing edge of the nozzle plays an important role during the primary atomization close to the nozzle orifice.

Measurements of droplet size and velocity were carried out at various atomizing pressures, liquid flowrates, nozzle geometries along radial and axial distances from the atomizer. The radial profile of the SMD at lowest air pressure was almost flat and the SMD value in the entire radial profile mainly in spray center decreases considerably with increasing

the air pressure. The liquid flow rate variation leads to a slight increase of the droplet size and a small decrease of the droplet velocity in the central region

Fig. 18. Effect of (a) prefilming area and (b) atomization edge length on the GSMD

of the spray. The maximum volume flux appears in ALR 1.28 at the spray center region. The axial direction measurement results reveal that the maximum droplet velocity and minimum droplet size is generated in 20 mm and 90-110 mm distance from the nozzle centerline exit in most operational conditions. The parameters influencing this important position have been identified. The GSMD was dependent on liquid flowrate with GSMD ~ $\dot{V_l}^{0.1}$, $\dot{V_l}^{0.16}$ and $\dot{V_l}^{0.18}$ for air pressures of 0.5, 1 and 1.5 bar. However, the air pressure dependency was GSMD ~ $P_{air}^{-0.82}$, $P_{air}^{-0.82}$ and $P_{air}^{-0.68}$ for liquid flowrates of 10, 50 and 150 ml/min, respectively. It was observed that increasing liquid flowrate reduces the dependency of air pressure on the GSMD in airblast atomizers. Finally, increasing the atomization edge length rises surprisingly the GSMD in low air pressure conditions, however, from an air pressure of 0.4 bar, droplet size decreases significantly with increasing the atomization edge within N3, N5 and N6. It was observed that an increase of the atomization edge length from 8.33 mm to 14.11 mm leads to a GSMD decrease of maximum 70 %. The prefilming area contributed to the liquid droplets size in two unlike behaviors in the current atomizer design. It was observed that a large prefilming surface causes slower droplet velocity due to a large wake region in front of the atomizer, however, it reduces also the droplet size due to the formed thin liquid film

before liquid atomization. Consequently, N1 is able to produce faster and smaller droplets among the other studied atomizer designs.

In future studies, these experimental investigations will be extended regarding the influence of liquid properties like viscosity and surface tension on the spray characteristic. Based on these and the given results, correlations will be derived to predict the primary droplet properties for pre-filming coaxial airblast atomizers. Furthermore, an atomization model will be derived to predict SMD based on identified physics and the experimental observations presented. Eventually, the data presented in this report will be applied for validating numerical air-blast atomization models which are currently under development.

ACKNOWLEDGEMENTS

REFERENCES

Albrecht, H. E., Damaschke, N., Borys, M. and Tropea, C. (2013). *Laser Doppler and phase Doppler measurement techniques*. Springer Science & Business Media.

Aliseda, A., Hopfinger, E. J., Lasheras, J. C., Kremer, D. M., Berchielli, A., & Connolly, E. K. (2008). Atomization of viscous and non-newtonian liquids by a coaxial, high-speed gas jet. Experiments and droplet size modeling. *International Journal of Multiphase Flow* 34(2), 161–175.

Arai, T., and Hashimoto, H. (1985). Behavior of Gas-liquid Interface on a Liquid Film Jet : Instability of a Liquid Film Jet in a Co-current Gas Stream. *Bulletin of JSME* 28(245), 2652–2659.

Ashgriz, N. (2011). *Handbook of atomization and sprays: theory and applications*. Springer Science & Business Media.

Avulapati, M. M. and Rayavarapu Venkata, R. (2013). Experimental studies on air-assisted impinging jet atomization. *International Journal of Multiphase Flow* 57, 88–101.

Babinsky, E. and Sojka, P. E. (2002). Modeling drop size distributions. *Progress in Energy and Combustion Science* 28(4), 303–329.

Berthoumieu, P. and Lavergne, G. (2001). Video techniques applied to the characterization of liquid sheet breakup. *Journal of Visualization* 4(3), 267–275.

Bhayaraju, U. C. (2007). *Analysis of liquid sheet breakup and characterisation of plane prefilming and nonprefilming airblast atomisers*. Technische Universität Darmstadt.

Correa, S. M. (1993). A Review of NOx Formation

Under Gas-Turbine Combustion Conditions. *Combustion Science and Technology* 87(1–6), 329–362.

Crapper, G. D. andDombrowski, N. (1984). A note on the effect of forced disturbances on the stability of thin liquid sheets and on the resulting drop size. *International Journal of Multiphase Flow* 10(6), 731–736.

Dantec Dynamic A/S. (2014). *BSA Flow Software User Guide* (5.20). Skovlunde, Denmark: Publication no.: 9040U5742.

Dombrowski, N. and Fraser, R. P. (1954). A Photographic Investigation into the Disintegration of Liquid Sheets. *Philosophical Transactions of the Royal Society of London. Series A, Mathematical and Physical Sciences* 247(924), 101–130.

Dombrowski, N. and Johns, W. R. (1963). The aerodynamic instability and disintegration of viscous liquid sheets. *Chemical Engineering Science* 18(3), 203–214.

Engelbert, C., Hardalupas, Y. and Whitelaw, J. H. (1995). Breakup Phenomena in Coaxial Airblast Atomizers. *Proceedings of the Royal Society of London. Series A: Mathematical and Physical Sciences* 451(1941), 189 LP-229.

Eroglu, H. and N. Chigier (1991). Wave characteristics of liquid jets from airblast coaxial atomizers. *Atomization and Sprays* 1(4).

Gepperth, S., Koch, R. and Bauer, H. J. (2013). Analysis and comparison of primary droplet characteristics in the near field of a prefilming airblast atomizer. In *ASME Turbo Expo 2013: Turbine Technical Conference and Exposition* (p. V01AT04A002-V01AT04A002). American Society of Mechanical Engineers.

Gepperth, S., Müller, A., Koch, R., Bauer, H., Strömungsmaschinen, T. and Institut, K. (2012). Ligament and Droplet Characteristics in Prefilming Airblast Atomization Lechler GmbH , Metzingen , Germany 320(1975), 2012.

Glathe, A., Wozniak, G. and Richter, T. (2001). The influence of eccentricity on the performance of a coaxial prefilming air-assist atomizer. *Atomization and Sprays* 11(1), 21–33.

Guildenbecher, D. R., López-Rivera, C., & Sojka, P. E. (2009). Secondary atomization. *Experiments in Fluids* 46(3), 371–402.

Haenlein, A. (1932). Disintegration of a liquid jet. Retrieved from https://digital.library.unt.edu/ark:/67531/metadc63598/

Hagerty, W. W. and Shea, J. F. (1955). A study of the stability of plane fluid sheets. *J. Appl. Mech*, 22(3) 509–514.

Hardalupas, Y. and Whitelaw, J. H. (1994). The characteristics of sprays produced by coaxial airblast atomisers. *Journal of Propulsion and Power* 10(4), 453–460.

Jedelsky, J., Otahal, J. and Jicha, M. (2007). Effervescent atomizer: influence of the internal geometry on atomization performance. *21 Th ILASS - Europe Meeting* 1–6.

Lasheras, J. C., Villermaux, E., & Hopfinger, E. J. (1998). Break-up and atomization of a round water jet by a high-speed annular air jet. *Journal of Fluid Mechanics* 357, 351–379.

Leboucher, N., Laporte, G., Carreau, J. L. and Roger, F. (2007). Effect of the inner gas jet on annular liquid sheet atomization. In *Proc. of the 21st Annual Conf. on Liquid Atomization and Spray Systems*.

Lefebvre. (1989). *Atomization and Sprays*. Corp., New York. Taylor & Francis.

Lefebvre, A. H. and McDonell, V. G. (2017). *Atomization and Sprays, Second Edition*. CRC Press.

Lefebvre, A. H. and D. R. Ballal (2010). *Gas turbine combustion*. CRC Press.

Li, X. G. and Shen, J. H. (2001). Experiments on annular liquid jet breakup. *Atomization and Sprays* 11(5), 557–573.

Liu, H. F., Gong, X., Li, W. F., Wang, F. C. and Yu, Z. H. (2006). Prediction of droplet size distribution in sprays of prefilming air-blast atomizers. *Chemical Engineering Science* 61(6), 1741–1747.

Liu, H. F., Li, W. F., Gong, X., Cao, X. K., Xu, J. L., Chen, X. L., … Yu, Z. H. (2006). Effect of liquid jet diameter on performance of coaxial two-fluid airblast atomizers. *Chemical Engineering and Processing: Process Intensification* 45(4), 240–245.

Mansour, A. and Chigier, N. (1995). Air-blast atomization of non-Newtonian liquids. *Journal of Non-Newtonian Fluid Mechanics* 58(2–3), 161–194.

Mehring, C. and Sirignano, W. A. (2004). Capillary stability of modulated swirling liquid sheets. *Atomization and Sprays* 14(5).

Rangel, R. H. and Sirignano, W. A. (1991). The Linear and Nonlinear Shear Instability of a Fluid Sheet. *October* 10(3), 2392–2400.

Rayleigh, L. (1878). On the instability of jets. *Proc. London Math. Soc* 10(1), 4–13.

Rizk, N. K. and Lefebvre, A. H. (1980). The influence of liquid film thickness on airblast atomization. *Journal of Engineering for Power* 102(3), 706–710.

Rizk, N. K. and Lefebvre, A. H. (1983). Influence of atomizer design features on mean drop size. *AIAA Journal* 21(8), 1139–1142.

Rizk, N. K. and Lefebvre, a. H. (1985). Spray characteristics of spill-return atomizers. *Journal of Propulsion and Power* 1(3), 200–204.

Sellens, R. W. and Brzustowski, T. A. (1985). A

prediction of the drop size distribution in a spray from first principles. *Atomisation Spray Technology* 1, 89–102.

Stapper, B. E., Sowa, W. A. and Samuelsen, G. S. (1992). An experimental study of the effects of liquid properties on the breakup of a two-dimensional liquid sheet. *Journal of Engineering for Gas Turbines and Power* 114(1), 39–45.

Urbán, A., Zaremba, M., Malý, M., Józsa, V. and Jedelský, J. (2017). Droplet dynamics and size characterization of high-velocity airblast atomization. *International Journal of Multiphase Flow* 95, 1–11.

Weber, C. (1931). Zum Zerfall eines Flüssigkeitsstrahles. *ZAMM - Journal of Applied Mathematics and Mechanics / Zeitschrift Für Angewandte Mathematik und Mechanik* 11(2), 136–154.

Xue, Q., Battistoni, M., Powell, C. F., Longman, D. E., Quan, S. P., Pomraning, E., … Som, S. (2015). An Eulerian CFD model and X-ray radiography for coupled nozzle flow and spray in internal combustion engines. *International Journal of Multiphase Flow* 70, 77–88.

Yang, B., Cuoco, F. and Oschwald, M. (2007). Atomization and flames in LOX/H2-and LOX/CH4-spray combustion. *Journal of Propulsion and Power* 23(4), 763–771.

Zhou, W. X. and Yu, Z. H. (2000). Multifractality of drop breakup in the air-blast nozzle atomization process. *Physical Review E* 63(1), 16302.